DØ Note 3320
September 29, 1997

Luminosity Monitor Technical Design Report

Amy Lo, Chyi-Chang Miao, and Richard Partridge

This report describes the design of the Luminosity Monitor for the DØ upgrade. The functionality and operational principles are largely the same as for the Level 0 trigger built by the Brown group for Run I. A summary of the Level 0 design and performance can be found in *The Level 0 Trigger for the DØ Detector* (DØ Conf 94-1). The Brown group proposed a new Luminosity Monitor for the DØ Run II upgrade, as described in *A Proposal for the DØ Upgrade Luminosity Monitor* (DØ Note 2860). Key differences between the Run I and Run II designs are a new counter geometry, the use of fine-mesh photomultiplier readout, and modifications of the electronics for 396 ns operation. In the sections that follow, we describe the Luminosity Monitor Goals, Counter Design, Electronics Design, and Software Requirements.

1. Luminosity Monitor Goals

The primary purpose of the Luminosity Monitor is to make an accurate determination of the DØ luminosity. Secondary goals include providing diagnostic information regarding accelerator performance, identifying beam crossings with multiple interactions, and providing large η trigger coverage for diffractive and rapidity gap triggers. These goals are discussed in more detail below.

1.1. DØ Luminosity Measurement

Making an accurate measurement of the DØ luminosity is important for a broad range of physics analyses in the experiment. Various options for measuring the DØ luminosity were evaluated in the Luminosity Monitor Proposal, with the conclusion that accurately counting non-diffractive inelastic collisions remains the best technique for measuring the DØ luminosity.

The Run I luminosity error of 5.3% can be divided into two parts: a DØ contribution due to uncertainties in detector acceptance and efficiency (2.6%) and a non-DØ contribution due to uncertainties in the inelastic and diffractive cross section measurements made by E710 and CDF (4.6%). Our goal is for the DØ contribution to be less than 2% in Run II. The non-DØ contribution will presumably change when E811 publishes its cross section measurements, although the sign and magnitude of this change are not clear.

For Run II, the center-of-mass energy will increase to 2 TeV. At present, there are no measurements of the inelastic and diffractive cross sections at this energy. However, these cross sections vary logarithmically with the beam energy, so it should be possible to accurately extrapolate these cross sections to $\sqrt{s} = 2$ TeV using lower energy measurements.

An additional goal for Run II is to provide a more robust luminosity database so that it is easier to make an accurate determination of the luminosity for the various data samples used in physics analyses.

1.2. Accelerator Diagnostic Information

An important secondary goal is to provide diagnostic information regarding accelerator performance, including instantaneous measurements of luminosity and beam halo rates, fast measurement of the luminous profile, and a precise measurement of the beam optics from separated beam scans.

All of these measurements require precise time-of-flight measurement for charged particles hitting the Luminosity Monitor counters. From the time difference between hits on opposite ends of the detector we can determine the z coordinate of the interaction vertex: $z_v = \frac{1}{2}c(t_{-z} - t_{+z})$. The instantaneous luminosity is determined by counting beam crossings where $|z_v| < 100$ cm and applying multiple interaction corrections. Proton and anti-proton beam halo rates are obtained by counting beam crossings where $z_v \approx \pm 140$ cm, corresponding to a time difference for a particle to travel from one end of the detector to the other end. Our goal is to provide instantaneous luminosity and beam halo measurements of comparable quality to what was achieved in Run I.

The luminous profile can be quickly determined from the distribution of the time difference $t_{-z} - t_{+z}$. In addition to providing a quick determination of the collision point, the luminous profile can be used to determine the beam optics at the IR from a separated beam scan. By separating the beams varying amounts in the vertical and horizontal directions, it was shown in Run I that the β^* and focal points of the beams in the $x - z$ and $y - z$ planes can be determined from changes in the luminous profile. Our goal for Run II is to provide the capability of quickly making a separated beam scan with minimal involvement of DØ or accelerator experts. Further information on the separated beam scan technique can be found in *Measuring the Tevatron Optics with the DØ Collider Detector* (DØ Note 2966) and *Experiments with Separated Beams in Run I at the Tevatron Collider* (http://d0wop.fnal.gov/online/Analysis/LogLum/7P23.ps).

1.3. Multiple Interaction Detection

The ability of the Level 0 detector to identify multiple interactions proved to be quite useful in Run I. A number of triggers with large cross sections benefited by being able to select events that predominantly had only a single interaction. In addition, multiple interaction detection proved to be an extremely valuable aide in understanding the pileup effects at high luminosity for a variety of physics analyses.

In Run I, the Level 0 trigger electronics calculated the standard deviation of the time-of-flight measurements in the two counter arrays. These standard deviations were added in quadrature and used to define the value of the Multiple Interaction Flag, which was made available in time for the Level 1 trigger decision. Our goal is to have a multiple interaction detection efficiency comparable to what was achieved in Run I. To meet this goal, the Luminosity Monitor counters must have a time-of-flight resolution no worse than $\approx$ 250 ps. An additional goal is to provide Multiple Interaction Flags to the Level 1 trigger during 36 bunch operation of the Tevatron.

Note that identifying multiple interactions based on timing complements multiple interaction identification based on tracking. Vertices that are close together in space will often be separated in time. Tracking detectors are insensitive to interactions where most of the charged particles are at large $|\eta|$. Finally, track reconstruction is too slow to be useful in early trigger stages.

1.4. Forward Trigger Coverage

The fast time response and small number of channels makes the Luminosity Monitor well suited to providing the trigger with signals indicating the presence of forward beam jets. These signals were used in Run I to help trigger on events with forward rapidity gaps that were used in DØ's observation of hard color-singlet exchange. With the proposed addition of a forward proton spectrometer to the DØ upgrade, it is likely that the Luminosity Monitor counters will again serve as useful trigger elements. Our goal is to provide whatever trigger signals are found to be useful that can be constructed based on the detection of forward beam jets.

2. Luminosity Monitor Counter Design

The design of the Luminosity Monitor counters is based on meeting the above design goals while avoiding conflicts with other detectors. Among the considerations that led to the present design are:

- The readout must be able to operate in the magnetic field of the DØ solenoid.
- The counters are constrained to lie between the beam pipe and the Forward Preshower detector and must not extend more than 10 cm from the face of the EC cryostat.
- The counters must provide a time-of-flight resolution of 250 ps or better.
- The counters should maximize the acceptance for non-diffractive inelastic collisions to minimize uncertainty in this acceptance.
- The Luminosity Monitor should have sufficient segmentation to allow multiple interactions to be identified by the spread in time-of-flight measurements.

In this section, we describe the selection of a readout technology, the counter design, the acceptance of the Luminosity Monitor for detecting inelastic collisions, various environmental conditions that have the potential to affect the counters, simulation studies that model the behavior of the counters, and tests of prototype Luminosity Monitor counters.

2.1. Selection of a Readout Technology

A critical choice in the Luminosity Monitor counter design is the selection of a new readout technology to replace the photomultiplier tubes used in the Level 0 counters. Two readout options were discussed in the Luminosity Monitor Proposal: fine-mesh photomultipliers and wave-shifting fiber readout. Prototype counters were built employing both readout options. The fiber readout prototype was only able to achieve a 500 ps time resolution, while the fine-mesh photomultiplier prototype met our goal of 250 ps time resolution as described below. Furthermore, the rigidity of the readout fibers proved to be problematic in trying to build small detectors

designed to fit within the small space allocated for the Luminosity Monitor counters and there were concerns about the ability of the fibers to withstand that high radiation levels near the beam pipe. Based on these results, we have selected the fine-mesh photomultiplier readout option.

2.2. Counter Design

The Luminosity Monitor counter design consists of an array of 24 identical 5/8" thick BC-408 scintillator wedges arranged symmetrically about the beam pipe and mounted on the endcap cryostat. The layout of the counters is shown in Fig. 1 and their location on the DØ detector is shown in Fig. 2. Hamamatsu 1" diameter fine-mesh photomultiplier tubes are mounted directly on the face of the scintillator wedges. This unconventional placement of the photomultiplier tube is necessary to align the photomultiplier axis with the magnetic field and meet the tight space constraints.

The present design differs from the array of hexagonal counters described in the Luminosity Monitor Proposal. The original goal of the hexagonal design was to minimize the distance between the photomultiplier tube and the scintillator edges. However, in cosmic ray tests we found a substantial shift in time response for charged particles that pass through the scintillator directly underneath the photomultiplier. This effect, which is now well understood from our simulation studies, led us to redesign the counter geometry resulting in the wedge design shown in Fig. 1. Advantages of the wedge design include decreased radiation damage to the photomultiplier tubes, placement of the tubes in a region that minimizes mechanical interference with the beam pipe assembly and potential tracker cabling paths, and uniform counter occupancy that should improve multiple interaction detection and minimize photomultiplier aging.

In addition to our studies of the 24 wedge design described below, we have also made extensive studies of a similar design that segmented the detector into 32 identical 1" thick scintillator wedges. Results from these studies can be found in *Study of the Run II Luminosity Monitor Counter Design* (DØ Note 3319). The results for the 32 wedge design are very similar to the 24 wedge design; however, the 32 wedge design

required the purchase of additional photomultipliers and introduced complexities in the mechanical design due to the photomultipliers being wider than the scintillator wedges.

2.3. Luminosity Monitor Acceptance

Uncertainties in the Luminosity Monitor acceptance are expected to be the dominant DØ contribution to the luminosity error. The uncertainty in acceptance decreases as the acceptance approaches unity, so our goal is to maximize the pseudorapidity coverage by bringing the luminosity monitors as close as possible to the beam pipe, providing coverage over the region $2.7 < |\eta| < 4.5$.

For the dominant hard core process, the acceptance is found to be 0.980 ± 0.011. Including single diffractive and double diffractive processes, the uncertainty in the Luminosity Monitor acceptance is estimated to be 1.7%. A more complete description of the acceptance results and the method used to obtain them can be found in the Luminosity Monitor Proposal.

2.4. Environmental Considerations

There are a number of environmental factors that we have considered in the design of the Luminosity Monitor. The effects of the magnetic field, radiation damage, photomultiplier aging, and Helium permeability are discussed below.

Magnetic Field The Luminosity Monitor counters are located in a region where the magnetic field maps indicate a nearly axial magnetic field of $\approx$ 1 Tesla. We have selected fine-mesh photomultipliers for the Luminosity Monitor readout due to their unique ability to operate in large magnetic fields while maintaining the desirable characteristics of conventional photomultipliers in precision time-of-flight applications (high gain, low noise, fast risetime, and good quantum efficiency). These tubes are constructed from planar fine-mesh dynode layers separated by 1 mm gaps. Unlike conventional photomultipliers, the planar geometry does not require electrostatic focusing, greatly reducing the impact of magnetic fields. The tubes must be oriented

approximately axial with the magnetic field since the spiraling electrons will follow the magnetic field lines.

We have tested two 1" diameter Hamamatsu fine-mesh photomultipliers in the DØ test beam magnet. The relative gain as a function of magnetic field is shown in Fig. 3 and is in good agreement with Hamamatsu specifications. It is our understanding that the observed loss of gain at large magnetic fields is largely due to a decrease in the probability that an electron liberated from a dynode plane will make its way through one of the holes in the mesh. Thus, we do not expect the presence of a magnetic field to seriously degrade the number of primary photoelectrons that are amplified by the dynode chain, which is the dominant factor in determining the intrinsic time resolution for a scintillation counter.

We used the DØ test beam to verify that the time resolution for a scintillation counter with fine-mesh photomultiplier readout is largely immune to magnetic fields. Fig. 4 shows the measured time resolution versus magnetic field. We estimate that for a 1 Tesla magnetic field the time resolution is degraded by $16 \pm 16\%$. Further details regarding the test beam studies can be found in *Study of the Run II Luminosity Monitor Counter Design* (DØ Note 3319).

Radiation Damage The principle effect of large radiation doses on scintillation counters is to create color centers in the scintillator and photomultiplier window that absorb light and reduce the number of photoelectrons. Using the charged particle multiplicities obtained in our acceptance studies, we estimate a radiation dose of 300 kRad/fb^{-1} at the innermost edge of the scintillator and 25 kRad/fb^{-1} at the center of the photomultiplier tube (the radiation dose varies as $1/r^2$). At these radiation levels, we expect there to be some darkening of the scintillator closest to the beam pipe that may require the scintillator to be replaced every few fb^{-1} to avoid a loss in efficiency. We anticipate that replacing the scintillator wedges will be a relatively simple and inexpensive operation that can be performed during a typical summer shutdown. Figure 5 shows the effect of radiation on the glass window of the photomultiplier tube. Conventional Borosilicate glass shows a significant reduction in transmission efficiency after a 140 kRad radiation dose (Fig. 6 shows the emission

spectrum for the BC-408 scintillator we plan to use). To reduce the radiation damage to the photomultiplier tubes, we plan to use tubes with either UV glass or quartz windows.

Photomultiplier Aging Photomultipliers can show aging effects where the dynode gain decreases as a function of the total anode charge extracted from the tube. In conventional photomultipliers, aging effects typically are seen after several hundred Coulombs of anode charge. According to Hamamatsu, there is considerable variation in the aging of individual tubes, with some tubes showing an increase in gain while other tubes show a decrease in gain. Figure 7 shows an illustration of aging effects published by Hamamatsu.

We plan to set the tube gain so that we extract 1 pC of charge for a 1 MIP track. With this gain, we will reach the maximum rated anode current of 10 μA at the peak Run II luminosity of 2×10^{32}. This corresponds to an anode charge of 50 C/fb^{-1}, so we don't expect to see significant aging effects until after several fb^{-1} are acquired. Unlike radiation damage, where the loss of photoelectrons degrades the resolution and efficiency of the counter, there is some ability to compensate for the loss of gain due to aging by increasing the high voltage applied to the tube or amplifying the anode signal. We are also considering lowering the photomultiplier gain and placing preamplifiers on the Luminosity Monitor counters.

Helium Permeability The glass body of the fine-mesh photomultiplier tubes is permeable to Helium gas. Figure 8 shows the concentration of Helium gas in the photomultiplier tube as a function of time for tubes exposed to normal atmospheric concentrations of Helium. The levels of Helium shown in Fig. 8 are not sufficient to damage the tubes or affect the operation of the tubes in the Luminosity Monitor. Given the large quantities of Helium in close proximity, we are concerned that the concentration of Helium inside DØ may rise to a level sufficient to damage the photomultiplier tubes. We expect that it will be necessary to monitor the Helium concentration inside DØ and provide the ability to flush the photomultiplier enclosure with Nitrogen gas if necessary.

2.5. Simulation Studies

We have developed a program to simulate the operation of the Luminosity Monitor counters to help optimize the Luminosity Counter design. The simulation includes the generation of scintillation light, photon propagation in the scintillator, and the response of the photomultiplier tube. These studies are described in detail in *Study of the Run II Luminosity Monitor Counter Design* (DØ Note 3319). We have used this simulation program to understand and optimize the design of the Luminosity Monitor counters. In this section, we illustrate how these simulation studies were used to improve the time resolution of the counters by eliminating reflections off the far end surface of the scintillator.

The measured arrival time of a charged particle will depend on where the particle hits the counter. with hits near the photomultiplier appearing to be earlier than hits far from the photomultiplier. Since the position of the hit is unknown, the timing resolution is degraded. Figure 9 shows the distribution of photon propagation times for charged particles hitting the counter at various radii for a counter design with reflective wrapping on all sides. For small radii, there are two peaks in the arrival time distribution. The later peak corresponds to photons that propagate the length of the counter, reflect off the large radius end, and then propagate to the photomultiplier. This second peak can be eliminated by putting an absorber on the large radius end of the counter. as is shown in Fig. 10.

To demonstrate why the eliminating the later peak in propagation time improves the time resolution, it is instructive to examine the predicted photomultiplier output signal, shown in Fig. 11. We see that despite wide variations in the photon propagation distributions, the photomultiplier signals all have very similar shapes except for small timing offsets. It turns out that these timing offsets track the mean photon propagation time, so the mean photon propagation time is the only parameter that affects the timing. By eliminating the second peak in the propagation time distribution, we have greatly reduced the variation in the mean photon propagation time for the large fraction of charged particles that strike the counter at small radius. This has the effect of reducing the time uncertainty due to position dependence from 182

ps when the far end is reflecting to 158 ps when the far end is absorbing.

2.6. Prototype Counter Tests

We have built prototypes of the Luminosity Monitor counters and measured their properties in a cosmic ray test stand built by the Brown group. Figure 12 shows that the test stand has excellent time resolution (56 ps), enabling it to accurately predict the arrival time of a particle striking the counter being tested. The resolution of a prototype Luminosity Monitor wedge counter is shown in Fig. 13. As discussed above, the measured time depends on the position of the charged particle hit as shown in Fig. 14. Overlaid on the data points is the position dependence predicted by the simulation studies, showing excellent agreement between the simulation and data.

The time resolution expected for the Luminosity Monitor counters depends on the intrinsic time resolution of the counter, the effect of the magnetic field on the intrinsic time resolution, and the contribution to the resolution from the position dependence expected at the Tevatron. The intrinsic time resolution is estimated to be 154 ps by selecting cosmic rays that strike the counter within a small range of positions to minimize the position dependence. We estimated the 1 Tesla magnetic field degrades the intrinsic time resolution by $\approx$ 16%, with an additional 158 ps contribution to the resolution from the position dependence, yielding an expected time resolution for the Luminosity Monitor counters of 240 ps.

The light collection efficiency was also observed to have a strong position dependence. Figure 15 shows the number of photoelectrons as a function of position. It is not surprising that the number of photoelectrons collected increases significantly when the charged particle hit lies under the photomultiplier. Using the particle data book's benchmark of 1 photon for every 100 eV of energy deposit in plastic scintillator, we can predict the expected number of photoelectrons using our simulation program. Figure 15 shows that the simulations do a good job of predicting the position dependence of the number of photoelectrons and have roughly the right normalization.

Further information on the prototype counter tests and comparisons with the simulation studies can be found in *Study of the Run II Luminosity Monitor Counter Design* (DØ Note 3319).

3. Electronics Design

This section describes the electronics to be used in the luminosity monitor. We propose to minimize the design of new electronics at this time by modifying much of the existing Level 0 electronics for operation at 396 ns. The sections below review the present Level 0 electronics and the modifications required for Run II.

3.1. Level 0 Electronics Overview

A block diagram of the existing Level 0 electronics is shown in Fig. 16. The photomultiplier signals are brought to the platform and amplified using commercial NIM electronics. At this point, the electronics divides into a "FASTZ" and "SLOWZ" path.

In the FASTZ path, an analog sum of all the photomultiplier signals at each end of the detector is made using NIM electronics. The two analog sum signals are sent over RG-8 foam cable to the MCH where they are discriminated by constant fraction discriminators. The outputs of the discriminators are fed to the FASTZ module, which uses the time difference between these signals to determine the vertex position. A vertex position with $|z_v| < 97$ cm is taken to indicate the presence of a non-diffractive inelastic interaction and results in a logic pulse being sent to the scalers and rate meters used to record the luminosity. A modified version of the FASTZ module is used to identify beam crossings consistent with having proton or anti-proton beam halo particles traversing the detector.

In the SLOWZ path, the photomultiplier signal is fed to the QTAC module that performs charge integration and time-to-amplitude conversion. These analog signals are sent over coaxial ribbon cable to the L0ADC modules in the Level 0 VME crate in the MCH. The L0ADC modules digitize the analog signals, apply calibration and charge slewing corrections, and form the following quantities: N_{hit}, $\sum t_i$, $\sum t_i^2$, t_{min}, and t_{max}. The L0VTX boards use these quantities to calculate the average and standard deviation of the times from each end of the detector. The information from the two ends of the detector is then combined to calculate the SLOWZ vertex position and the multiple interaction flag.

3.2. Run II Modifications to the FASTZ Path

In Run I, commercial NIM modules were used to form an analog sum of the 20 Level 0 counters closest to the beam pipe. The timing of each PMT signal was adjusted using delay lines so that all signals were coincident within $\approx$ 100 ps. One problem with this approach is that a very large dynamic range is required. We want to be efficient for beam crossings with single particles hitting the detector, while avoiding saturation for the more typical beam crossing that might have several interactions and a large number of charged particles traversing the detector. We were unable to find a fully satisfactory compromise between full efficiency and avoiding saturation in Run I. For Run II, we plan to use a hybrid digital/analog technique for combining the PMT signals. Each PMT signal will be sent to a constant fraction discriminator that will provide a timing pulse with minimal charge slewing effects. The outputs of the constant fraction discriminators will then be used in the analog sum, limiting the dynamic range in the analog sum. Discriminating this signal at 50% of its maximum amplitude is expected to produce a timing signal that will track the median time of particles hitting the Luminosity Monitor counters. With this modification, we should be able to provide luminosity signals for either 396 ns or 132 ns bunch spacings.

3.3. Run II Modifications to the SLOWZ Path

The SLOWZ electronics path was designed to operate with 396 ns bunch spacing, but this mode of operation was never fully tested. We have begun the process of testing each component with 396 ns bunch spacing and understanding what modifications may be necessary to operate with this new timing. With the exception of the QTAC time-to-analog converters, no part of the SLOWZ path is expected to operate with 132 ns bunch spacing and will be scrapped at the end of 36 bunch operation.

Figure 17 shows the output of the QTAC time-to-amplitude converter operating with 396 ns bunch spacing where three different start times are overlaid. It is seen that the reset can be accomplished in under 50 ns providing the analog signal with $\approx$ 300 ns of settling time. In the near future, we will verify that the charge integration

circuit is able to operate with 396 ns bunch spacing and that the analog signals are sufficiently settled after traversing the ribbon coax to the MCH.

The L0ADC boards have sample-and-hold circuits that acquire the analog signals, which are then multiplexed to the input of a flash ADC. The ability of the digitization section of the ADC boards to operate with 396 ns bunch spacing has already been demonstrated since digitization was completed within 300 ns in Run I. The digital section of the ADC board is pipelined with no stage of the pipeline taking more than 396 ns.

The present L0ADC board is not designed to provide the event buffering required to operate in Run 2. While sufficient buffers exist on the board, the logic for controlling which buffers are filled and which buffer is enabled for readout needs to be modified. We believe this problem can be circumvented by allowing a redesigned VME controller to directly drive the event buffer address pins, but the details of how this is done remain to be worked out. Another change is that the timing pattern for the 24 on-board clock signals will need to be completely different. We expect that it will be possible to implement the new timing by downloading different timing patterns, but given the complexity of the L0ADC timing it is possible that additional hardware changes may be required.

The L0VTX boards are entirely digital with the input and output signals latched to provide the necessary pipelining. The event buffering and clock patterns will require the same changes required for the L0ADC boards.

3.4. New VME Controller Board

A new VME controller board will be designed to provide the interface between the Luminosity Monitor ADC and VTX boards and the Run II trigger and buffering scheme. It is anticipated that the new controller will make use of unused pins on the VME backplane to directly control which buffers in the ADC and VTX boards are being filled with new data and which buffer is being readout by the VBD.

3.5. Luminosity Scalers

To record the luminosity and livetime for the various trigger and deadtime conditions, a substantial number of scalers are being incorporated into the trigger framework. The Luminosity Monitor will provide signals indicating the presence of a non-diffractive inelastic interaction from both the FASTZ and SLOWZ path. In addition, scalers will count the number of beam halo hits. Further information on the scalers used by the Luminosity Monitor can be found in *Run II Scalers for DØ* (DØ Note 3149).

3.6. Plans for 132 ns Bunch Spacing

We expect to continue to provide luminosity signals using the FASTZ path when the accelerator changes to 132 ns bunch spacing. Although the SLOWZ path will be scrapped, we will continue to want the Luminosity Monitor timing and pulse height information recorded in the raw data stream and are exploring how this might be done. While providing multiple interaction flag bits to the Level 1 trigger is beyond the scope of our current plans, we expect to retain the ability to calculate these flags in software from the timing and pulse height data in the raw data.

4. Software Requirements

A variety of software components are required for the Luminosity Monitor. In this section, we give a brief description of the software components and their function.

4.1. Monte Carlo Software

The Luminosity Monitor counters were added to the DØGSTAR Monte Carlo by Jeff Bantly before he left Brown. Code still needs to be added to convert the hits to the Luminosity Monitor data format. In addition, a minor update will be required when the mechanical design is completed.

4.2. Online Software

Online software components include downloading, monitoring, and calibration packages. The downloading package is needed to initialize the Luminosity Monitor electronics. As in Run I, hardware consistency checks will be performed in the Level 3 unpacking routines. Appropriate histograms for shift monitoring will be incorporated in the Run II equivalent of the Run I Trigger Examine. We will continue to rely on data for the Luminosity Monitor calibration, but plan to accumulate the necessary calibration data using the online system to avoid the lengthy turn-around time we encountered last run when we used offline data.

4.3. Offline Software

The offline reconstruction code largely consists of unpacking and making available Luminosity Monitor calculations stored in the raw data block. Luminosity Monitor routines need to be added to the event display program to facilitate debugging and physics analysis. In addition, it may again be useful to develop a Multiple Interaction Tool that combines the Luminosity Monitor timing information with the charged particle tracking information.

4.4. Luminosity Recording

A variety of software components are needed to record and extract the luminosity. Online software is required to make the luminosity available to various monitoring programs used by DØ and accelerator operations. We plan to use a database to store the various pieces of information needed to calculate the integrated luminosity for a given data sample. Online routines are needed to retrieve the appropriate information and save it in the database, while offline routines will be needed to extract the integrated luminosity for the various datasets being used for physics analysis. A new feature planned for Run II is to incorporate the instantaneous luminosity in the raw data so that the instantaneous luminosity is always kept with the event.

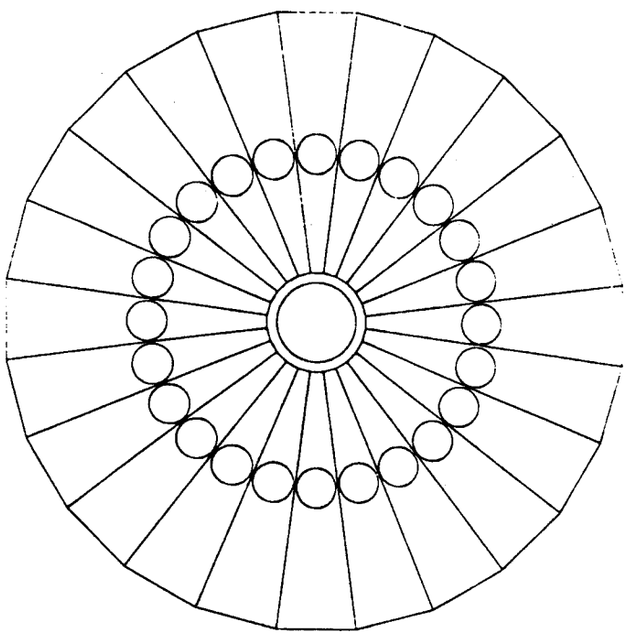

Figure 1: Schematic drawing of the Run II Luminosity Monitor design showing 24 wedge counters surrounding the beam pipe with fine-mesh photomultiplier tubes mounted on the face of each wedge counter.

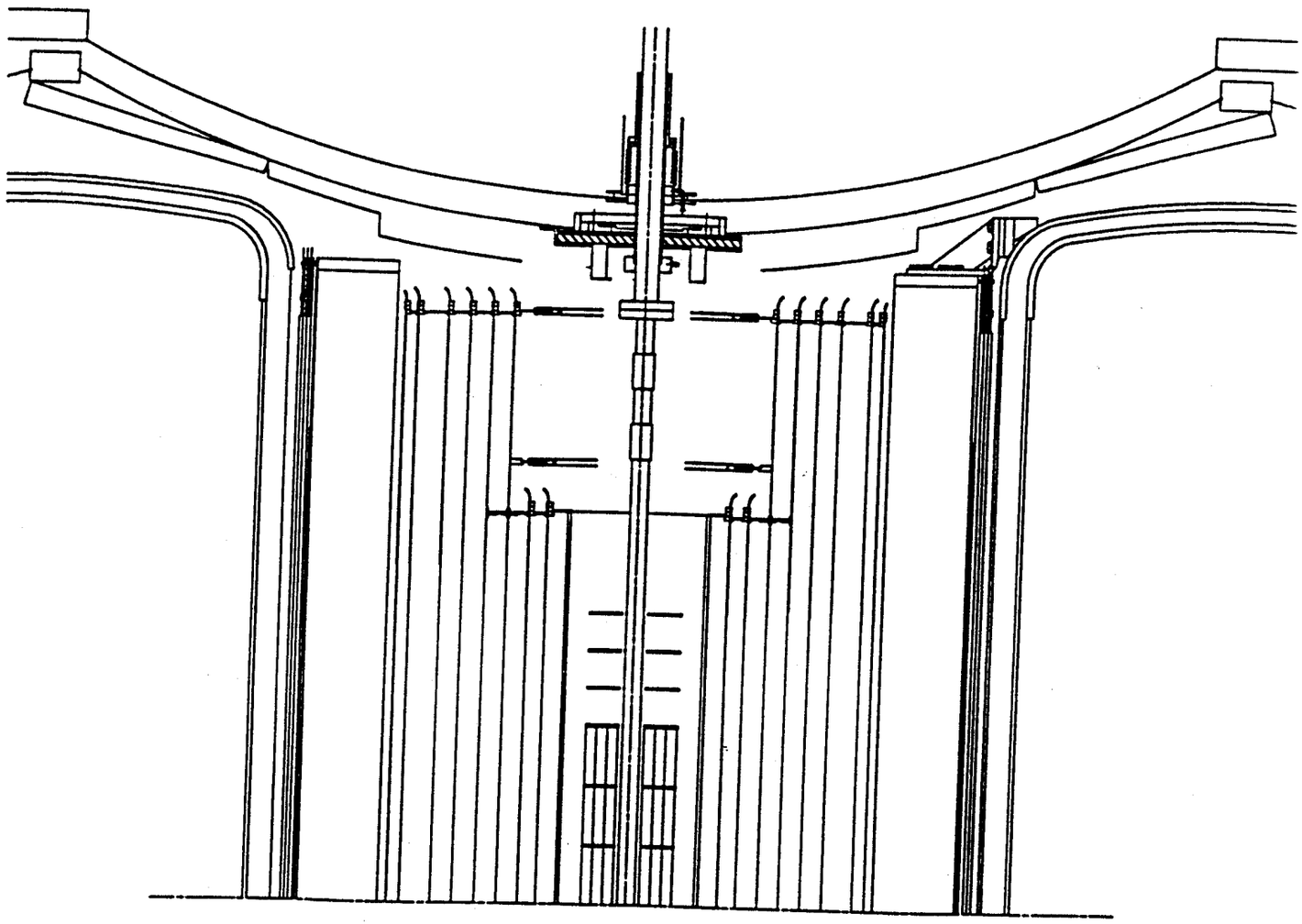

Figure 2: Side view of the Luminosity Monitor mounted on the face of the EC cryostat.

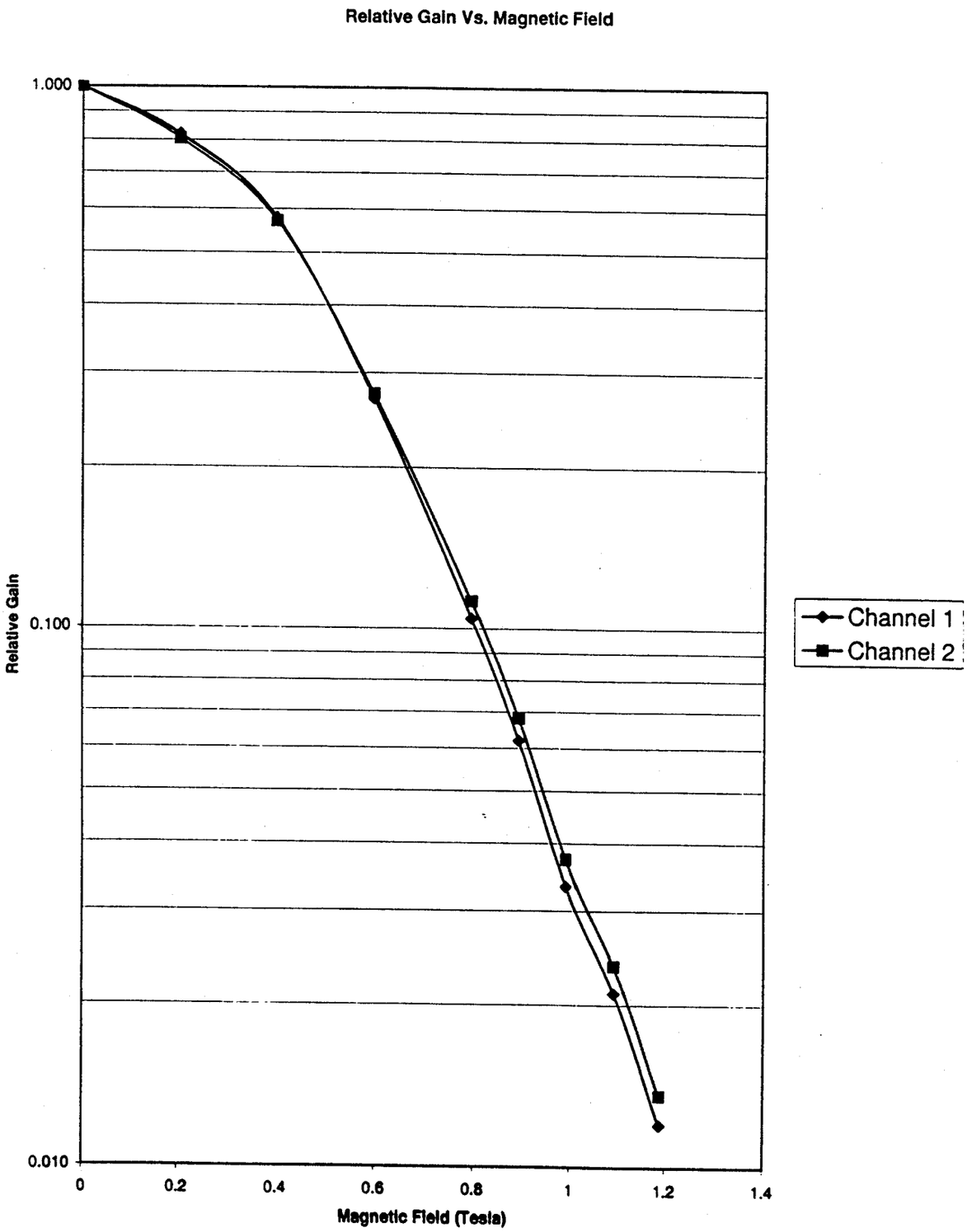

Figure 3: Relative gain versus magnetic field for two 1" diameter fine-mesh photomultiplier tubes.

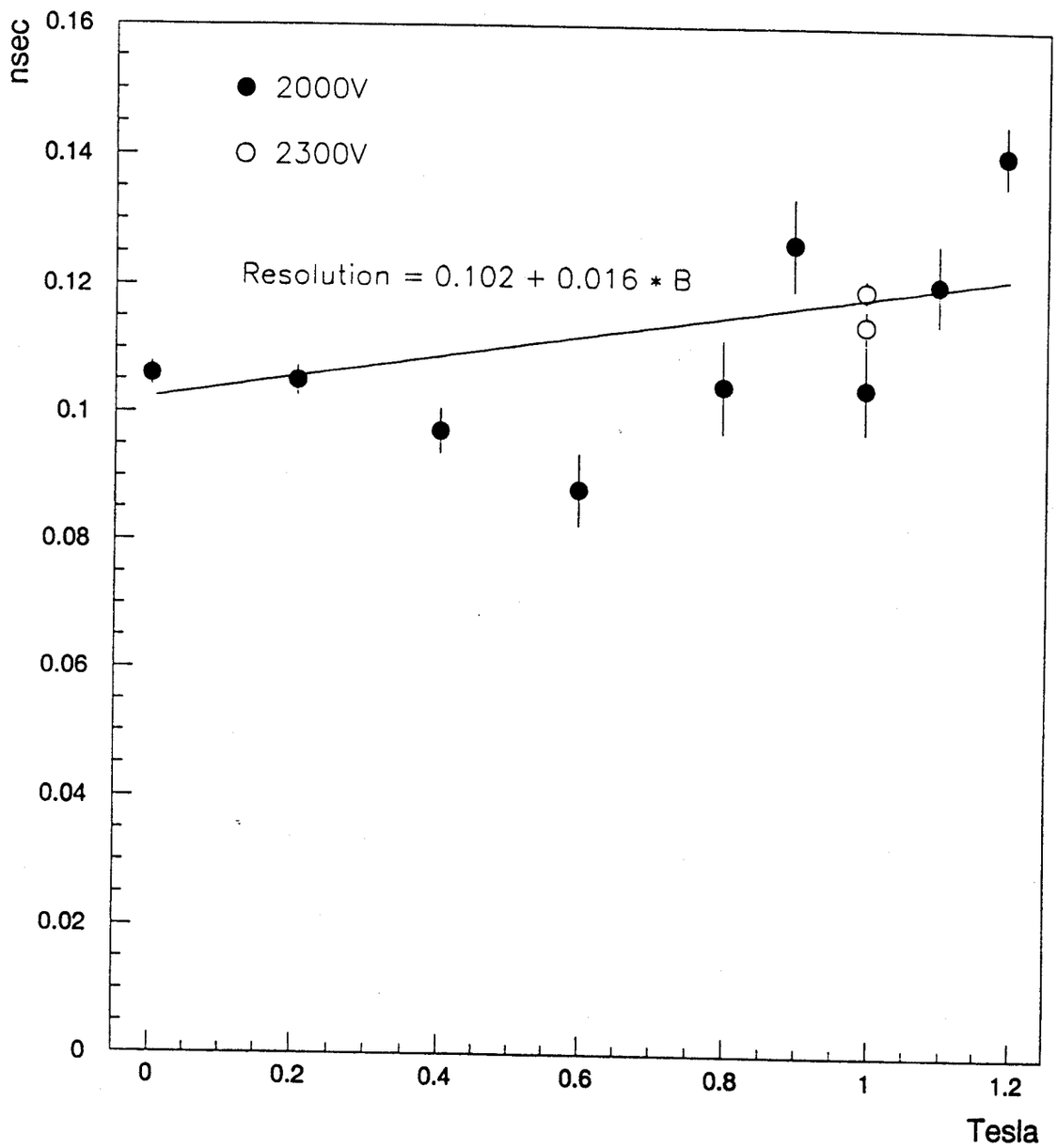

Figure 4: Time resolution versus magnetic field for test counters with fine-mesh photomultiplier readout.

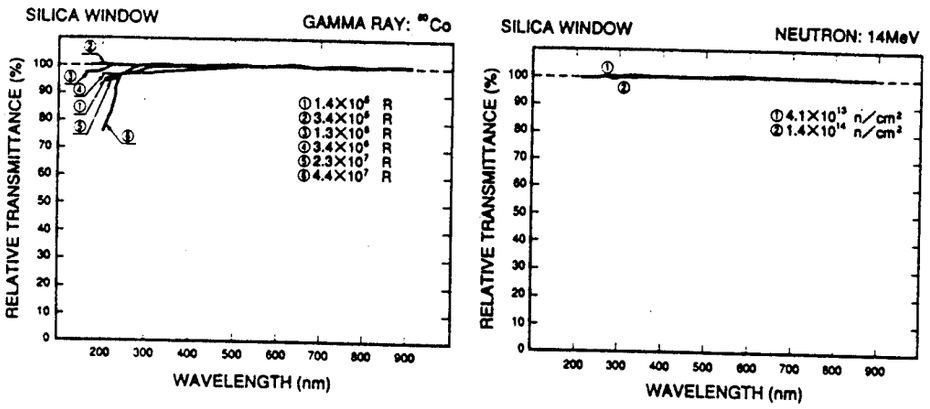

TPMOB0022EA

Figure 8-11: Transmittance variations of a synthetic silica window when irradiated by gamma rays and neutrons

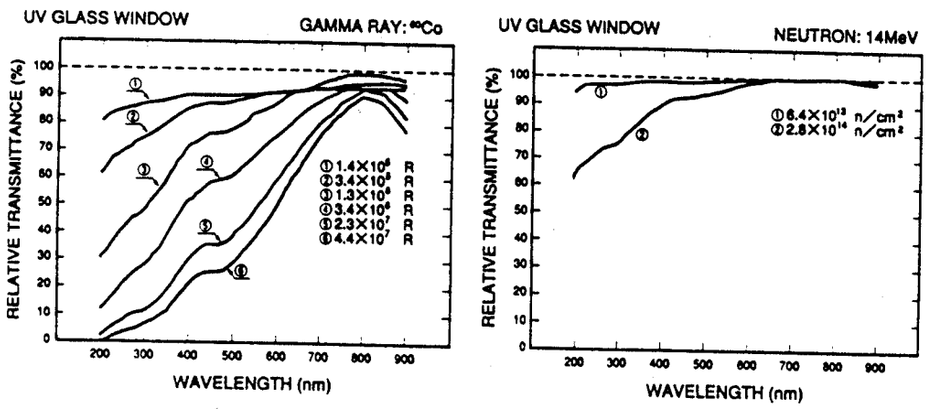

TPMOB0023EA

Figure 8-12: Transmittance variations of a UV glass window when irradiated by gamma rays and neutrons

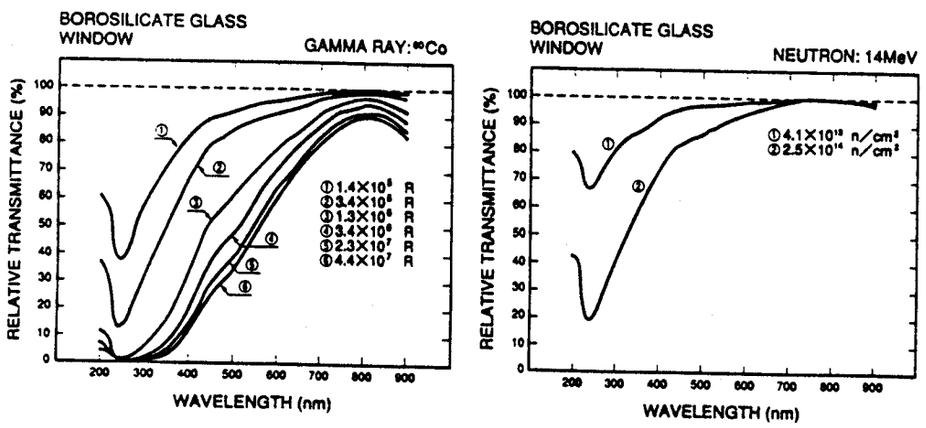

Figure 5: Effect of radiation on light transmission through a photomultiplier window.

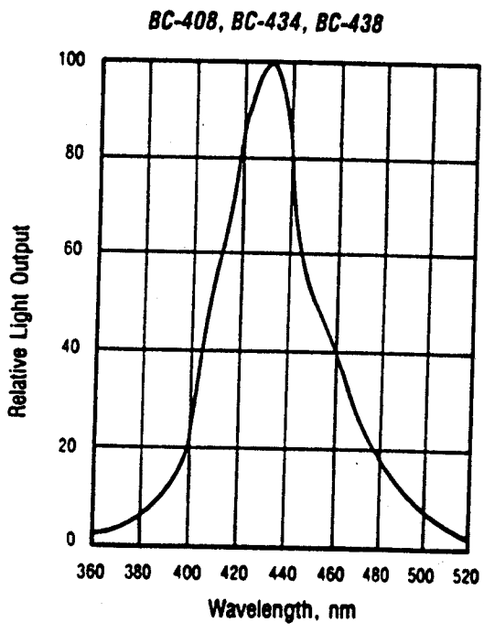

Figure 6: Emission spectrum for Bicron BC-408 plastic scintillator.

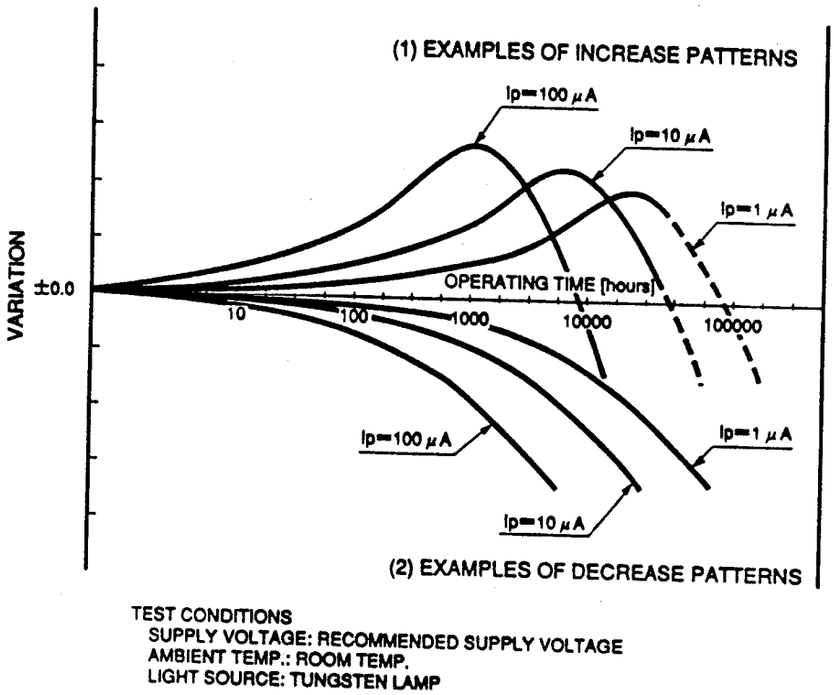

Figure 7: Examples of photomultiplier aging for Hamamatsu photomultipliers.

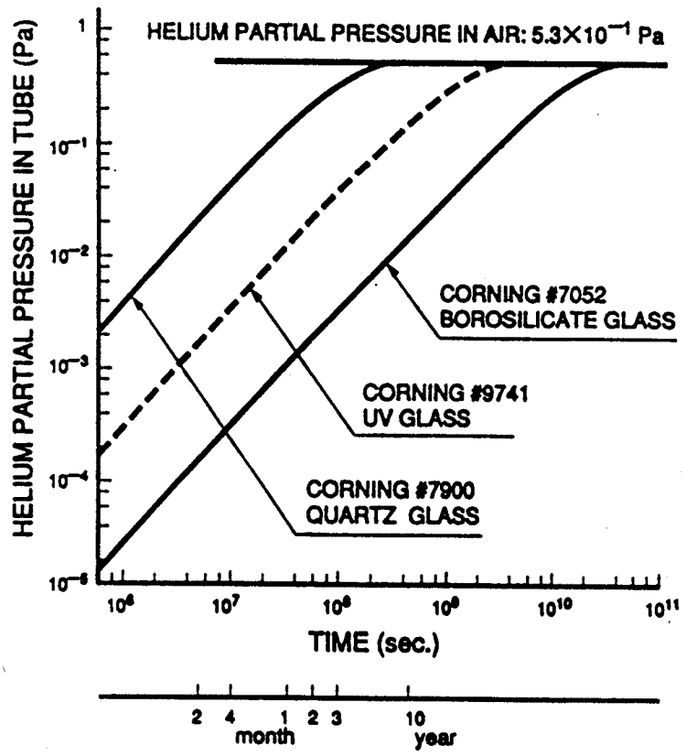

Figure 8: Helium gas concentration inside a photomultiplier versus time.

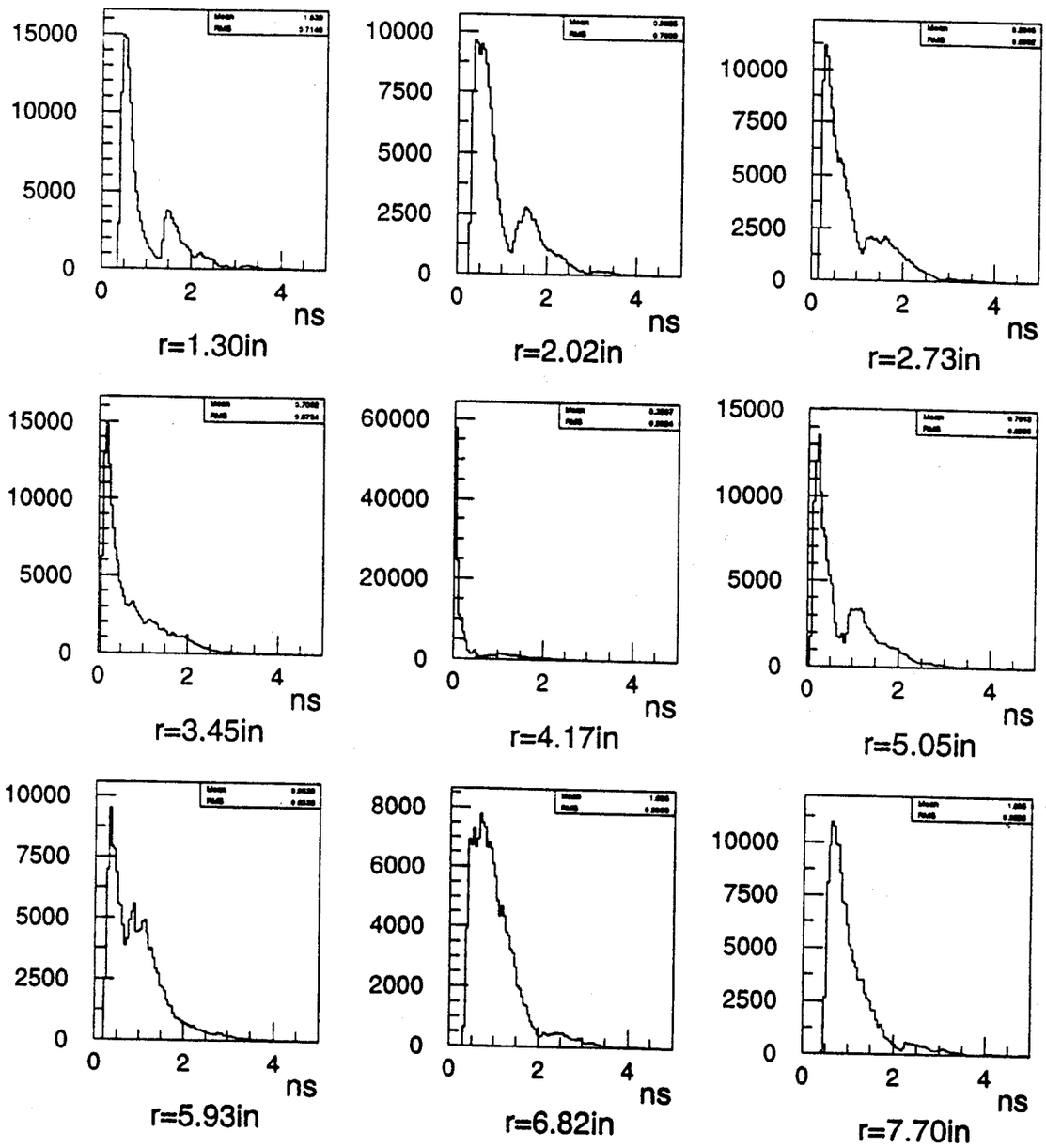

Figure 9: Distribution of photon propagation times for charged particle hits at various radii (with reflector on outside scintillator edge).

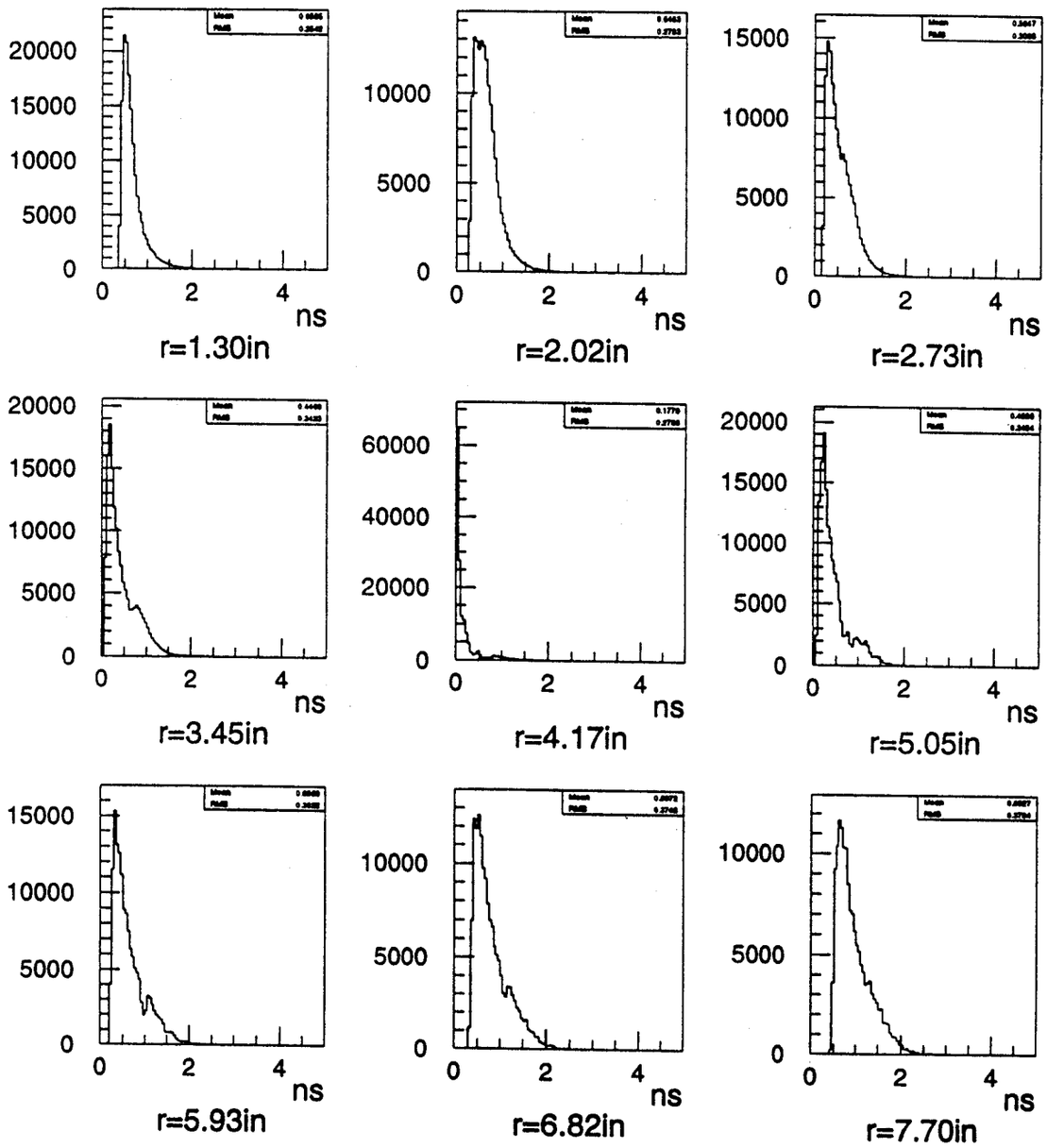

Figure 10: Distribution of photon propagation times for charged particle hits at various radii (with absorber on outside scintillator edge).

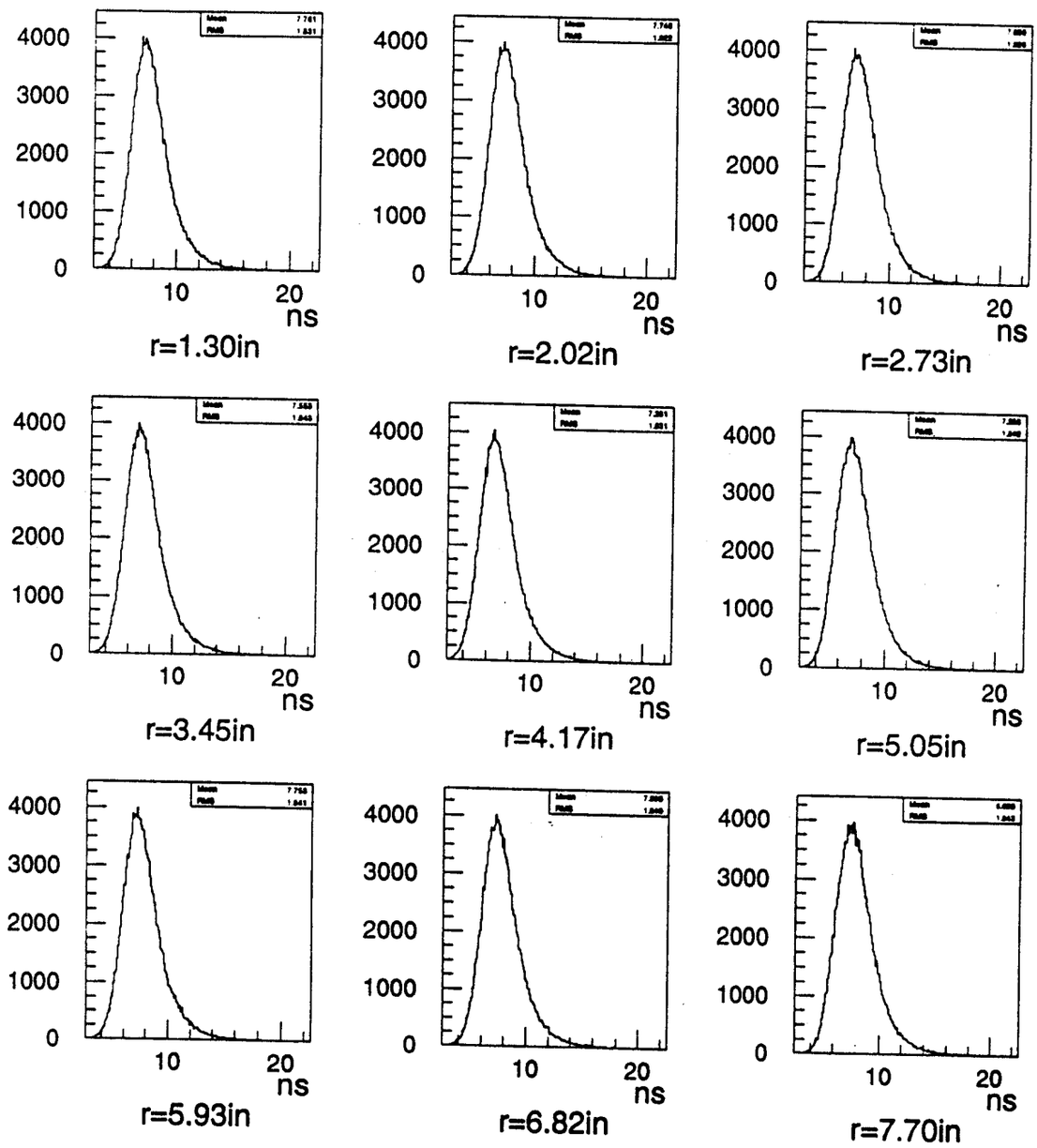

Figure 11: Predicted photomultiplier pulse shape for charged particle hits at various radii (with absorber on outside scintillator edge).

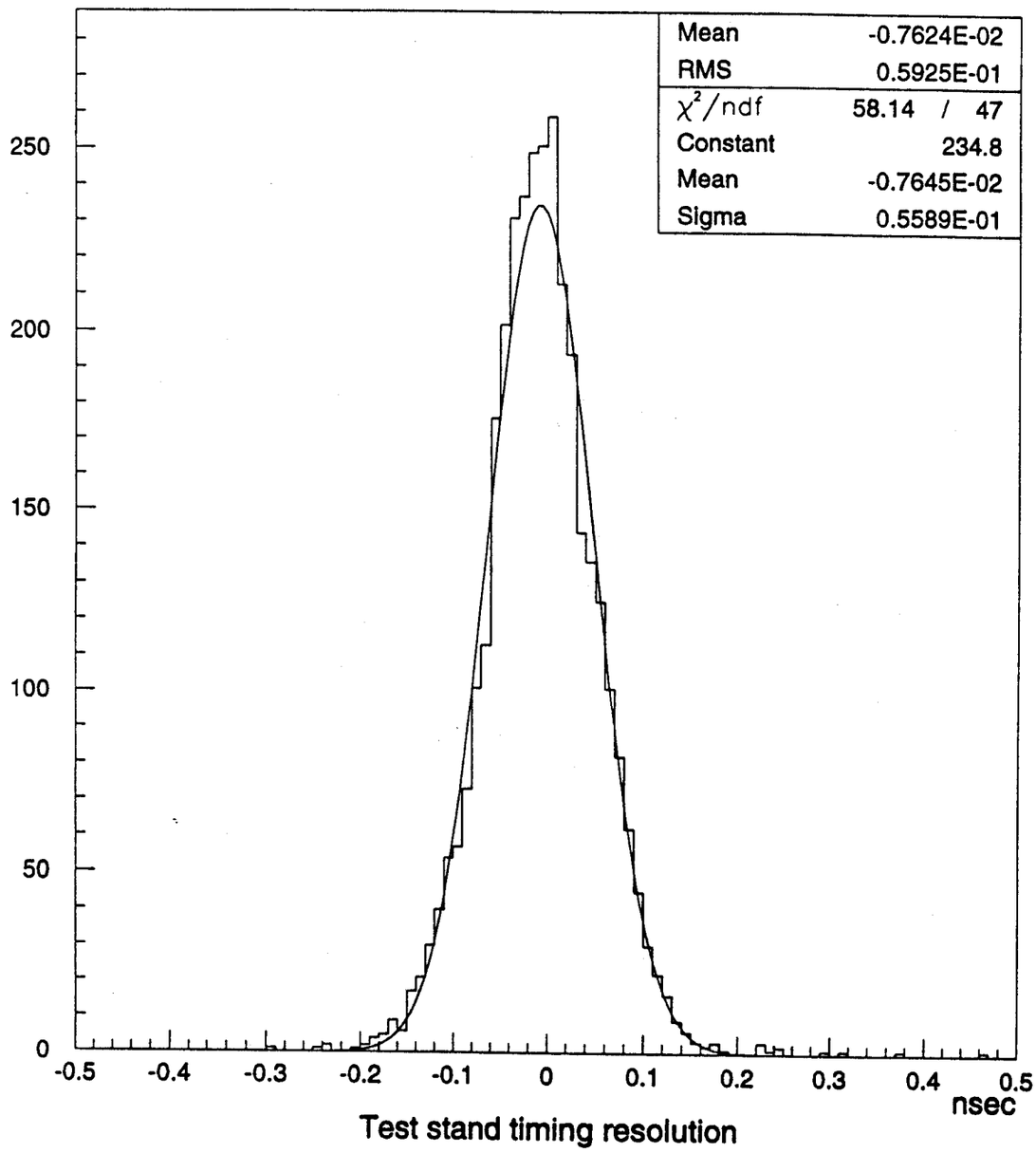

Figure 12: Time residual for cosmic ray test stand. The width of this distribution measures the time resolution of the test stand.

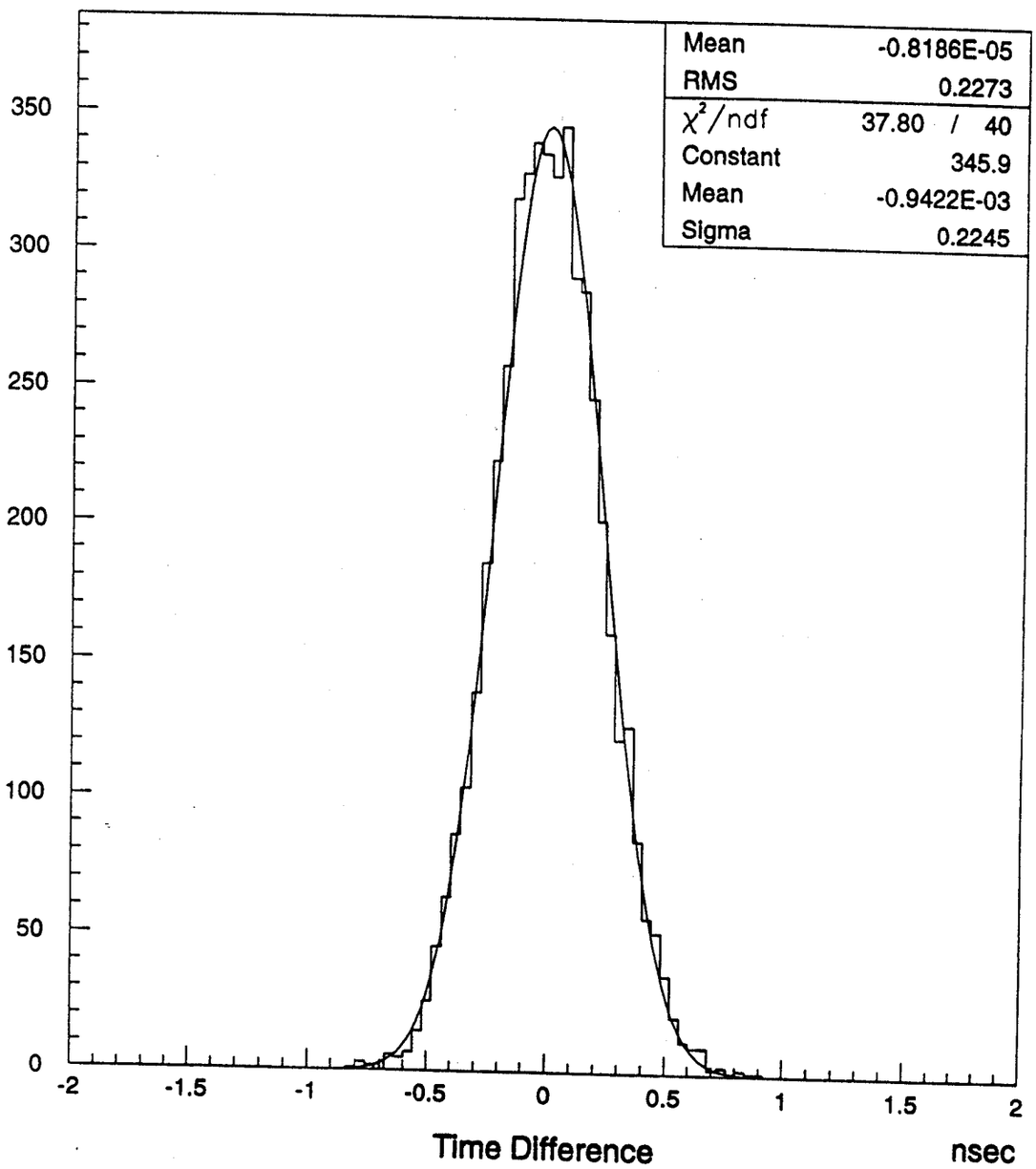

Figure 13: Difference between the measured and predicted arrival times showing the resolution for a prototype Luminosity Monitor counter.

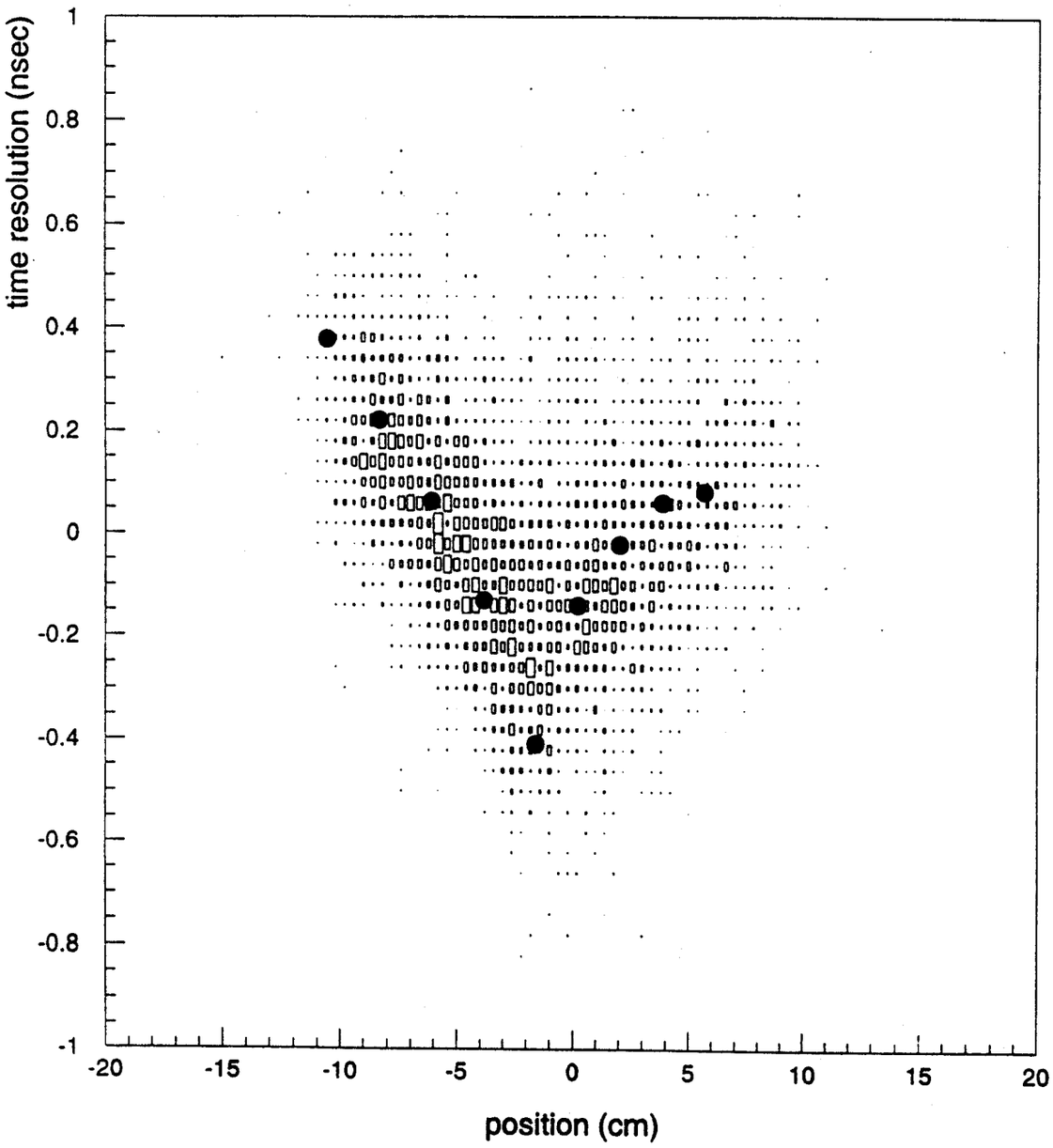

Figure 14: Difference between the measured and predicted arrival times versus charged particle hit position for a prototype Luminosity Monitor counter. The points show the predicted position dependence from the simulation studies. The origin of the position axis is underneath the photomultiplier with positive positions closer to the beam axis.

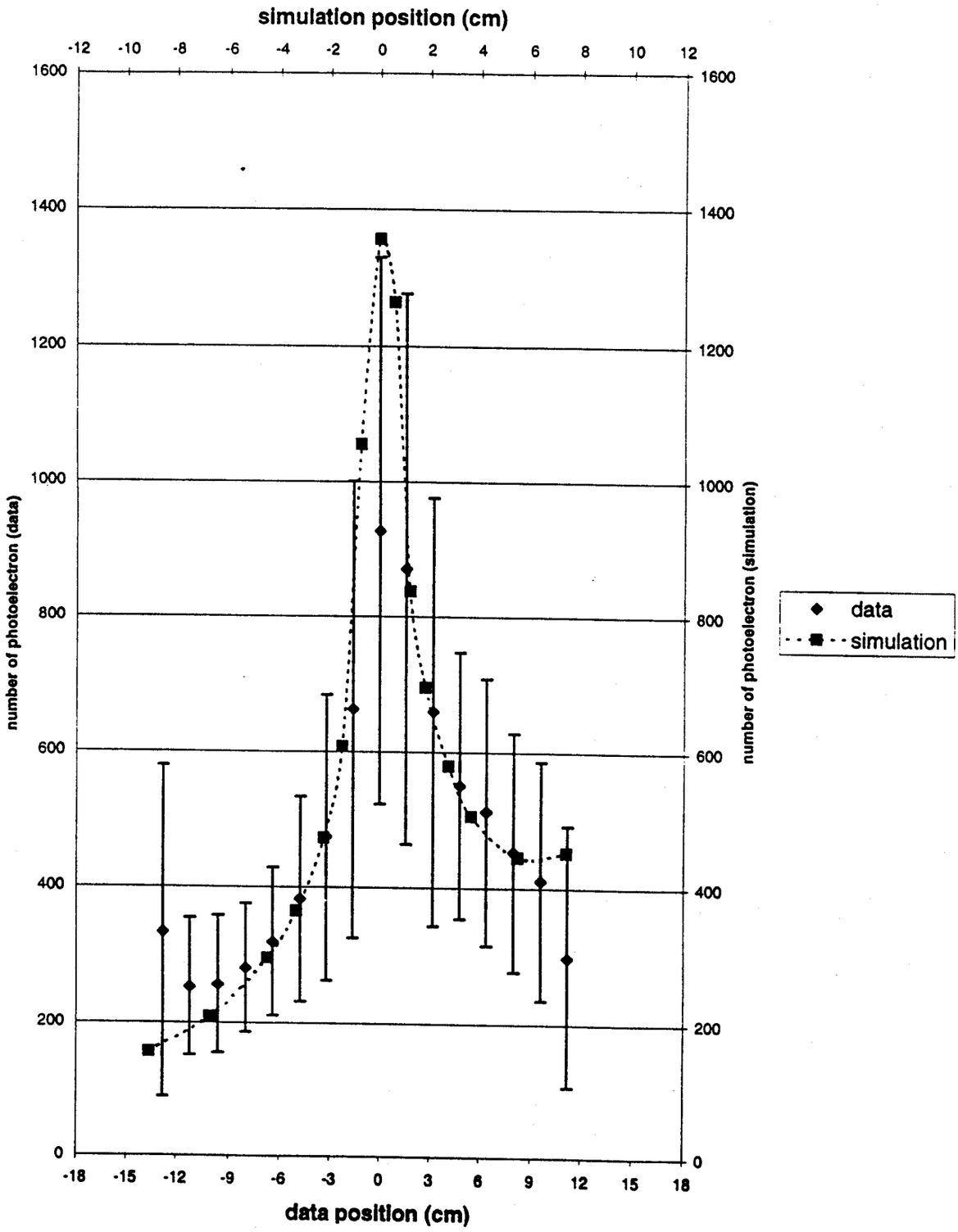

Figure 15: Number of photoelectrons versus charged particle hit position. The points show the predicted number of photoelectrons from the simulation studies. The origin of the position axis is underneath the photomultiplier with positive positions closer

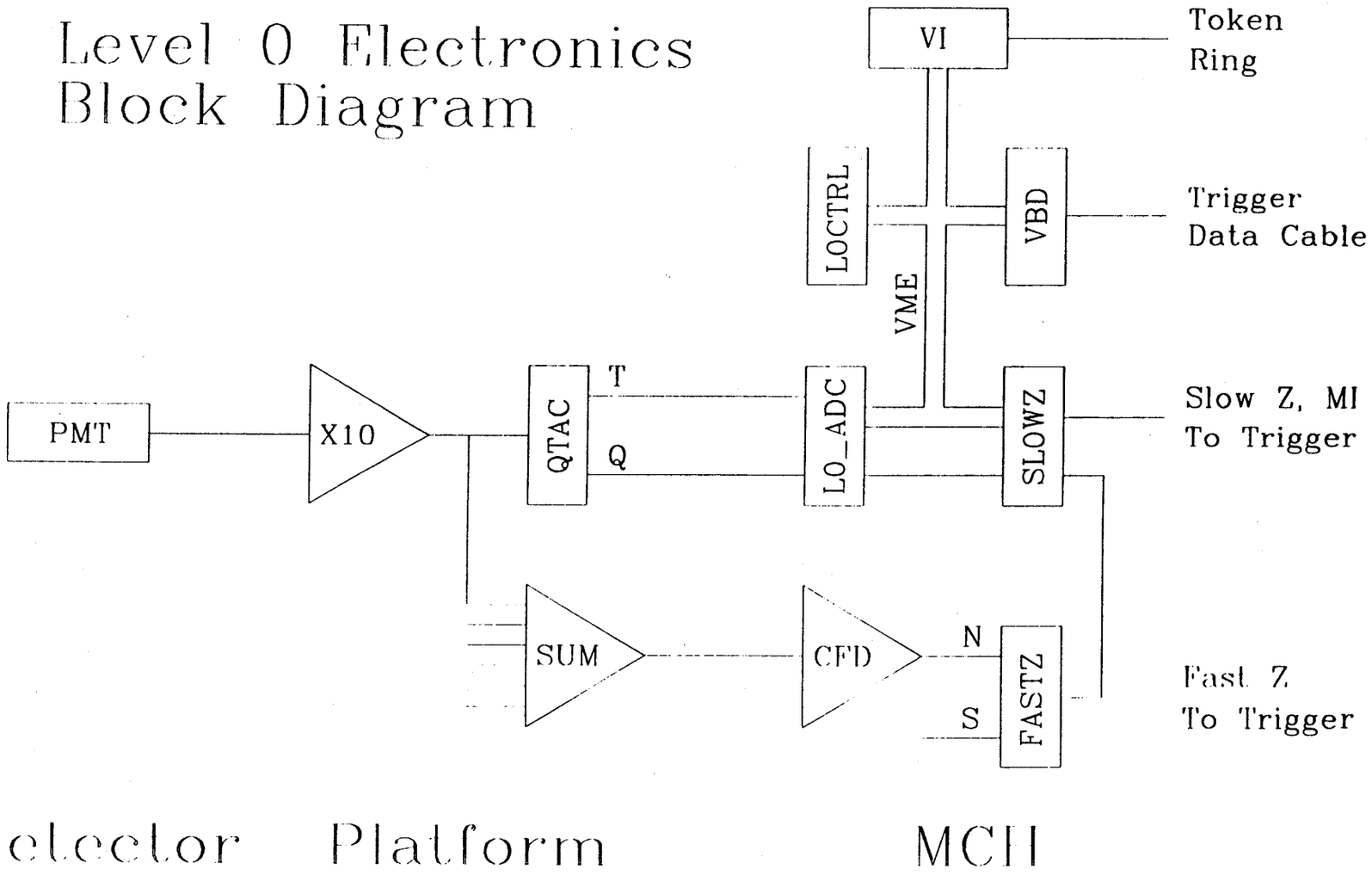

Figure 16: Block diagram of the Run I Level 0 electronics.

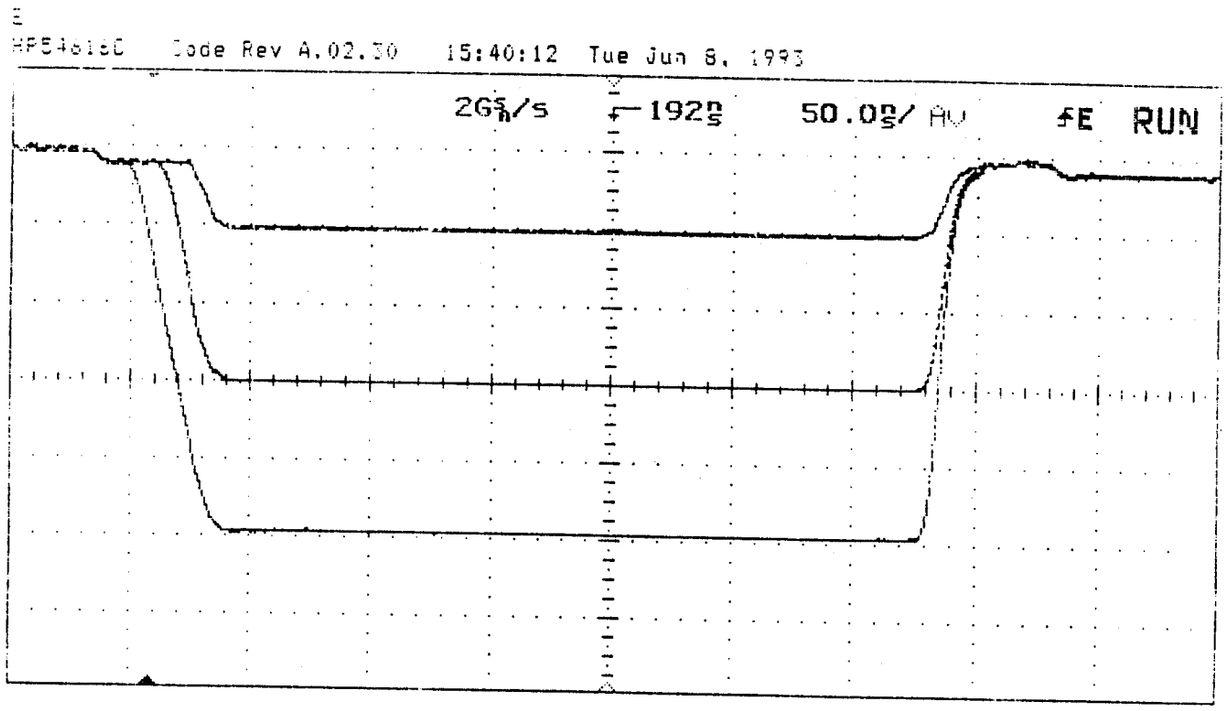

	State	Volts/Div	Position	Cplg	BW Lim	Inv	Probe	Input
Chan 1	Off	1.000 V	-2.031 V	DC	Off	Off	10:1A	1M
Chan 2	Off	500.0mV	0.000 V	DC	Off	Off	1:1A	50
Ext	---	---	---	DC	---	---	1:1A	50

	Mode	Main Time/Div	Main Delay	Time Ref	Delayed Time/Div	Delayed Delay
Horizontal	Normal	50.00ns/	192.0ns	Cntr	--------	-----

Trigger	Mode	Source	Level	Holdoff	Slope	Couplg	Reject	NoiseRej
	Normal	Ext	-468.8mV	300.0ns	Pos	DC	Off	Off

Display Mode: Average # Average: 256

Trace Labels (Displayed Traces)
56 ns Saved: 15:30:42 Tue Jun 8, 1993
89 ns Saved: 15:33:36 Tue Jun 8, 1993
32 ns Saved: 15:35:22 Tue Jun 8, 1993

Figure 17: Time-to-Amplitude converter output operating with 396 ns bunch spacing. Three different start times are shown corresponding to 3 ns, 16 ns, and 29 ns between the start and stop signals.